Journal of the Optical Society of America B
OPTICAL PHYSICS

SOA fiber laser mode-locked by gain modulation

B. N. Nyushkov,[1,2,3] S. M. Kobtsev,[1,*] A. K. Komarov,[4] K. P. Komarov,[4] and A. K. Dmitriev[2,3]

[1]Novosibirsk State University, Novosibirsk 630090, Russia
[2]Institute of Laser Physics, Siberian Branch of Russian Academy of Sciences, Novosibirsk 630090, Russia
[3]Novosibirsk State Technical University, Novosibirsk 630073, Russia
[4]Institute of Automation and Electrometry, Siberian Branch of Russian Academy of Sciences, Novosibirsk 630090, Russia
*Corresponding author: sergey.kobtsev@gmail.com

Received 27 July 2018; revised 27 August 2018; accepted 28 August 2018; posted 29 August 2018 (Doc. ID 340909); published 24 September 2018

This work reports, for the first time to our knowledge, on an experimental and theoretical study of mode locking via synchronous pumping of a semiconductor optical amplifier (SOA) used as the active medium of a fiber laser. SOA modulation with injection current pulses having duration of 1.2 μs and repetition rate equal to that of the fundamental intermode frequency spacing of the cavity (84.9 kHz) led to generation of mode-locked pulses with duration of 650 ns at a wavelength of 1.54 μm. The feasibility of the proposed method and the basic parameters of the generated pulses are corroborated by numerical modeling. The key advantages of the proposed laser are simplicity of implementation, comparatively high efficiency, spectral universality, and possibility of pulse shape control.

https://doi.org/10.1364/JOSAB.35.002582

1. INTRODUCTION

Gain switching/modulation technologies (or synchronous pumping where switching/modulation frequency is a multiple of the cavity-free spectral range) are broadly used for generation of pulsed laser radiation [1–5]. Their main advantage consists in relatively simple implementation, since no special modulators or saturable absorbers are necessary. It is even easier to use these technologies without external seed pulses; in this case, the output pulses are formed directly by gain switching/modulation. The shortest pulse duration achievable through gain switching/modulation largely depends on the lifetime of the upper level of the laser's active medium, which can differ by more than an order of magnitude in various gain media [6]. Within the fiber laser domain, gain switching/modulation is successfully and efficiently implemented in Yb and Tm lasers [7–12] featuring relatively short lifetime of the upper laser level: 0.7–1.3 ms for Yb, depending on Yb ion concentration and the host glass [13], and 0.3 ms for Tm [11]. However, these technologies are not used in Er-doped fiber lasers because of a much longer lifetime of erbium ions on the upper laser level (10 ms) [14].

In general, gain switching/modulation delivers considerably better energy efficiency of pulsed generation compared, for example, to other mode-locking approaches, since pulsed pumping reduces energy consumption and improves generation efficiency by more than an order of magnitude (ratio of average output power of the laser radiation to the electric power consumption by the pump laser). Such highly energy-efficient technologies are important in applications with significant power/energy limitations, for instance, in space-based or mobile laser systems.

The present work for the first time, we believe, reports application of energy-efficient gain switching/modulation to generation of laser pulses in the vicinity of 1.5 μm on the basis of a hybrid laser including a semiconductor optical amplifier (SOA) as the gain medium and a fiber-optical resonator (SOA fiber laser). Such a laser essentially unites semiconductor and fiber optical technologies and may be referred to as "semiconductor fiber laser" or, in short, "semifiber laser". Unlike conventional Er-doped fiber active media, an SOA features significantly faster response times amounting to <25 ps [15]. At the same time, the broadest available gain bandwidth of SOA exceeds the gain profile of the Er-doped fiber active medium and may reach up to 120 nm [16]. The main demerit of semifiber lasers is their limitation on the output pulse energy (or average output power) due to inability of the current SOA to withstand relatively high energy/power of incident radiation, which is, conversely, accessible with Er-doped fiber media. Saturation power of the best currently available SOA may only reach about +22 dBm [17]. Nevertheless, as the results discussed in the following sections indicate, semifiber lasers represent a highly competitive alternative to fiber lasers for generation of pulsed laser output with comparatively low average power within the range of tens of milliwatts. Additionally, semifiber laser technology is spectrally universal because the working spectral range of various SOAs covers wavelengths [18,19] inaccessible with conventional fiber-active media.

2. EXPERIMENT

The layout of the proposed SOA fiber laser is schematically shown in Fig. 1.

The ring-linear cavity of the laser includes a commercially available fiber-coupled C-Band SOA (Thorlabs SOA 1013S) and a fiber circulator ensuring unidirectional generation in the 2.4-km long ring part of the cavity (normal-dispersion Corning MetroCor fiber). This circulator also forms the linear arm of the cavity, where a fiber Bragg grating (FBG) is installed for output wavelength selection and stabilization. A fused 50% coupler was inserted into the ring part of the cavity in order to extract radiation. The SOA was pumped electrically through a current controller driven by an arbitrary waveform generator (Rigol DG4162). The reflection spectrum of the FBG was approximately 1-nm-wide and centered at 1539.7 nm, the reflection coefficient being 0.95. A long resonator used in this work reduces its intermode frequency to below 100 kHz and, correspondingly, relaxes the speed requirements to the SOA current controller, which must be modulated at the cavity intermode spacing frequency. A longer cavity also allows higher per-pulse energy at the same average power. The latter frequency was 84.9 kHz in the studied configuration.

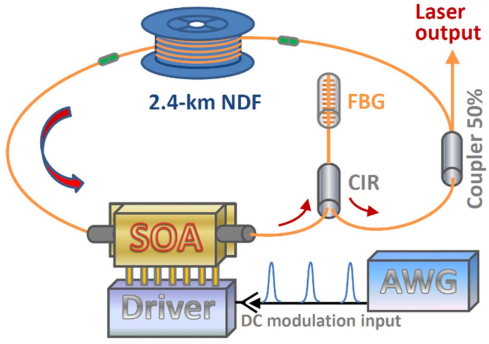

Fig. 1. Studied SOA fiber laser: SOA, semiconductor optical amplifier in the form of fiber-pigtailed component; NDF, normal-dispersion fiber; CIR, fiber circulator; FBG, fiber Bragg grating; AWG, arbitrary waveform generator; Driver, current controller with DC (direct current) coupled modulation input.

For mode locking of the studied semifiber laser, the SOA was modulated with 1.2-μs-long current pulses at a repetition rate of 84.9 kHz and 100% depth of modulation. The duration of pump current pulses was limited by the speed of the SOA current controller. It should be noted also that relaxation processes in the SOA develop within a subnanosecond time scale. Since we used relatively long current pulses, the SOA relaxation dynamics could not significantly affect laser pulse formation.

Mode-locked operation required relatively precise matching of the control pulse frequency to the intermode cavity frequency: detuning of the pumping pulse frequency by more than 1 kHz led to reduction of the average output power by 30 dB. The highest observed mode-locked average output power was 1 mW, with the pulse energy being 12 nJ.

Shown in Fig. 2 is a mode-locked pulse train, as well as shapes of both electric control pulse and the generated optical pulse. It can be seen that the generated 650-ns-long optical pulse is shorter than the corresponding electrical control pulse. It is pertinent to note that the observed output pulse duration is not the shortest possible for the mode-locking method used. In this work, rather than trying to achieve the fastest output, we limit ourselves to demonstration of the feasibility of mode locking in SOA fiber lasers through gain switching/modulation. We believe that the proposed method holds a significant potential of much shorter pulses, provided that faster electronic control hardware is used. This is the goal of our continued studies. By taking into account the picosecond speed of SOAs, it is reasonable to expect that the proposed method can be used to achieve output pulses in the picosecond duration range.

Figure 3 compares the optical spectra of the studied laser in CW generation regime (SOA pumped with constant current) and in mode-locked operation. As shown, mode locking leads to substantial broadening of the radiation spectra reaching 0.5 nm. This amounts to half the FBG reflection bandwidth and corresponds to the earlier identified pattern for mode-locked fiber lasers [20], where the output pulse spectrum is half as wide as the bandwidth of the intracavity spectral selector.

Additionally, we registered the radio-frequency (RF) spectrum of intermode beat signal of the semifiber laser in mode-locked regime with a fast photodetector and an RF spectrum analyzer. The observed spectrum (Fig. 4) was typical of

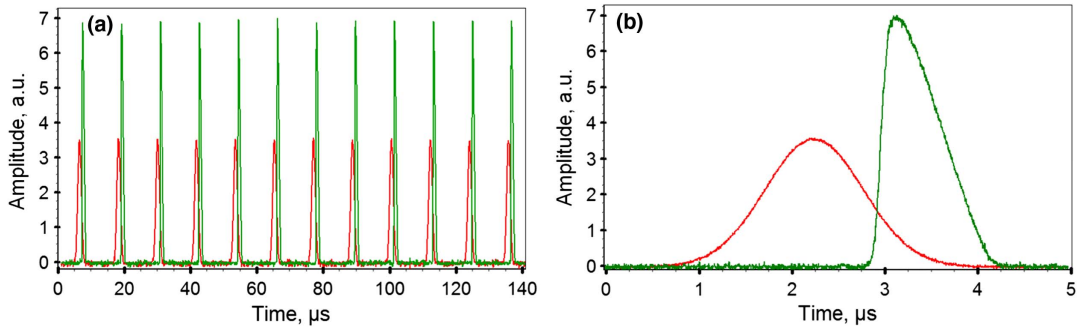

Fig. 2. (a) Time traces of electric control pulses (red curves) and generated laser pulses (green curves): regular pulse train with the fundamental repetition rate of 84.9 kHz; (b) one pulse selection from the pulse train. The traces were acquired by means of a Keysight DSO-X 3052T oscilloscope.

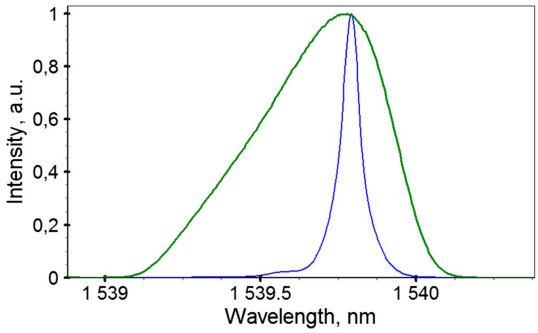

Fig. 3. Output radiation spectrum of the semifiber laser in mode-locked (green curve) and CW (blue curve) operation. The spectrum was measured by a YOKOGAWA AQ6370 optical spectrum analyzer with resolution of 0.02 nm.

mode-locked lasers, featuring a broad stable comb of peaks equidistantly spaced at the intermode frequency with relatively high signal-to-noise ratio of all its components.

It was interesting to explore the theoretic possibility of shaping the envelope of the generated laser pulses by respective shaping of the electric pulses modulating the SOA gain. This was reasonable to expect because of comparatively fast SOA response. An experimental confirmation of this possibility is demonstrated in Fig. 5.

Figure 5 shows that M-shaped control pulses lead to generation of similar M-shaped laser output. Duration of such laser pulses was nearly 1.3 times shorter than duration of the control pulses. This lower ratio between the durations of control and laser pulses (as compared with the initial ratio of ~1.9 obtained with Gaussian-shaped control pulses) could be due to different pulse shaping dynamics inside a fiber cavity for two widely different temporal profiles of gain modulation. Nevertheless, the demonstrated possibility of laser pulse shaping by corresponding shaping of electric control pulses opens up new prospects in the production of pulses with arbitrary tailored shape.

3. THEORY

Generation properties of a hybrid semifiber laser were modeled according to the following description, taking into account successive cyclic passes of the laser pulse through the passive cavity fiber, semiconductor amplifier, spectral filter, and coupler where the pulse loses some of its energy. The evolution of the field during its propagation through the fiber in the reference frame of the moving pulse is governed by the following dimensionless equation [21]:

$$\frac{\partial E}{\partial \zeta} = iD_i \frac{\partial^2 E}{\partial \tau^2} + iqIE, \tag{1}$$

where $E(\zeta, \tau)$ is the electric field amplitude, τ is the dimensionless temporal variable normalized to δt (the scale δt is chosen

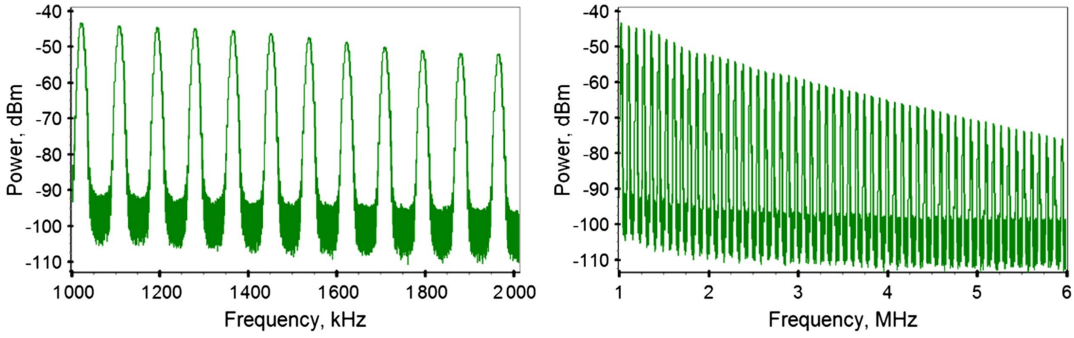

Fig. 4. RF spectra of intermode beat signal of the mode-locked semifiber laser. The spectra were measured by a ROHDE&SCHWARZ HMS-X RF spectrum analyzer with a resolution bandwidth of 10 kHz.

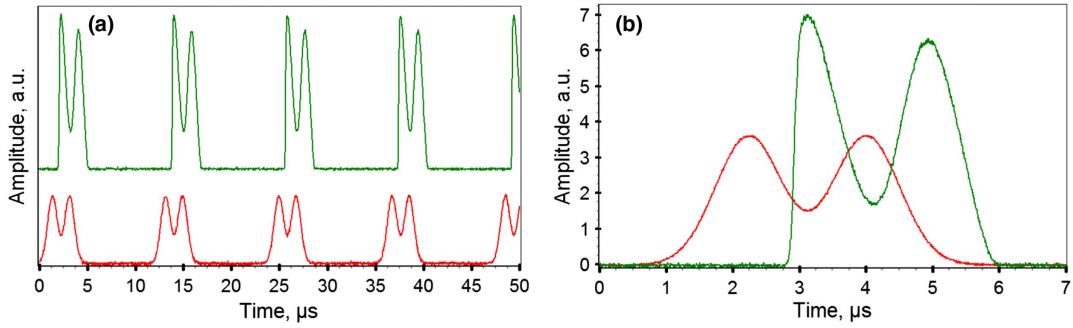

Fig. 5. (a) Time traces of M-shaped electric control pulses (red curve) and generated laser pulses (green curves): regular pulse train with the fundamental repetition rate of 84.9 kHz; (b) one pulse selection from the pulse train. The traces were acquired by means of a Keysight DSO-X 3052T oscilloscope.

for convenience of numerical modeling), ζ is the normalized distance travelled by the pulse (number of cavity round trips), D_i is the dimensionless frequency dispersion of the fiber medium refractive index ($D_i = \frac{L\beta_2}{2\delta t^2}$, where L is the fiber length, β_2 is the dimensional frequency dispersion of the fiber medium group velocity), $I = |E|^2$ is the intensity normalized to I_0, which, by the order of magnitude, is close to the value of $(\gamma L)^{-1}$, where $\gamma(\mathrm{W}^{-1}\,\mathrm{m}^{-1})$ is the dimensional nonlinearity of the refractive index. When dimensionless intensity I is defined in this manner, the value of parameter q is in the vicinity of unity. Variation of q allows modeling of the field evolution in the fiber at different values of refraction index nonlinearity without changing the value of I_0. Using the split-step Fourier method [22,23] for Eq. (1), we find the relationship between the fields before and after the fiber.

The pulse amplification upon passing through the semiconductor amplifier is given by the expression

$$g = \frac{a}{1 + bI(\tau)} \exp[-(\tau/d)^2], \tag{2}$$

where a is the pump parameter, b is the gain saturation parameter ($b = I_0/I_s$, where I_s is the dimensional saturation intensity of the semiconductor amplifier), and $2\sqrt{\ln 2}d$ is the dimensionless duration of the pump pulse. Since the analyzed pulses have microsecond durations and the relaxation time of population inversion in the semiconductor lies in the nanosecond range [15], the dependence of the gain coefficient g on the field intensity I is held to be instantaneous. We also neglect the effects of spectral filtration of radiation inside the amplifier, since the gain bandwidth of the utilized amplifier exceeds ~70 nm, whereas the transmission bandwidth of the filter used is only around ~1 nm. Accordingly, the linewidth enhancement factor is the same for all spectral components of the pulse and is equal to 1. The evolution of the field in the amplifier is given by the equation $\partial E/\partial\zeta = gE$. Using the Runge–Kutta method [24], from this equation we find the relationship between output and input fields for arbitrary pump value a.

The modification of the radiation intensity upon passing of the laser pulse through the frequency filter is given by the following super-Gaussian dependence of the filter transmittance upon the frequency detuning of the incident radiation ω from the central transmission frequency of the filter:

$$T = \exp[-\ln 2(2\omega/\Delta\omega)^{2n}], \tag{3}$$

where $\Delta\omega$ is the width of the transmission contour of the filter at half magnitude. Parameter n was calculated from the experimental dependence of the filter transmittance $T = T(\omega)$: $n = \frac{\Delta\omega}{2\ln 2}\frac{dT}{d\omega}$ at $\omega = \Delta\omega/2$. For a spectral filter, the relationship between the spectral components of the input and output pulses has the form: $E_{\omega\mathrm{out}} = \sqrt{\mathrm{TE}_{\omega\mathrm{in}}}$.

When the pulse propagates through the coupler, its intensity is reduced by a factor of $1/(1-\sigma_0)$, where σ_0 is the fraction of the radiation energy coupled out of the cavity. Parameter σ_0 can also be used to take other linear cavity losses into account. Here, the amplitudes of the input and output pulses are related by $E_{\mathrm{out}} = \sqrt{1-\sigma_0}E_{\mathrm{in}}$.

The numerical procedure starts from the evaluation of the electric field after passing through the fiber, SOA, the filter, and the coupler. The computed output field is then used as the new input for Eq. (1). This iterative procedure is repeated until a steady state is achieved.

Numerical modeling was performed with parameters of Eqs. (1) and (2) close to the experimental parameters of the studied laser: $L = 2.4$ km, $\beta_2 = -0.01$ ps^2/m, $\gamma = 5\cdot10^{-3}$ W^{-1}m^{-1}, $\sigma_0 = 0.55$, $I_s = 21.4$ mW, $\delta t = 5$ ps, $I_0 = 139$ mW, $q = 1.65$, $D_i = -0.5$, $b = 6.5$, $\Delta\omega = 1$ nm, $d = 1.2\cdot10^5$ (pumping pulse duration of 1 μs), and super-Gaussian function parameter $n = 2$. The results of transient evolution modeling are presented in Figs. 6 and 7. The initial temporal distribution of the pulse had Gaussian shape with no phase modulation. A stationary intensity distribution was reached as soon as after ~10 cavity round trips. However, a stationary spectral distribution of the pulse was only observed after a much larger number of cavity round trips $\zeta \sim 10^5$. Approximately after 100 round trips, the initially bell-shaped spectral profile split into two peaks, the distance between which linearly increased with the number of field round trips through the cavity (see Fig. 7). In this process, a stationary spectral distribution of radiation was formed between these repealing peaks, whose intensity monotonically dropped with the number of round trips. When these peaks disappeared, the full stationary spectral distribution was reached. Figure 8 gives both temporal and spectral distributions of the steady-state generation pulse.

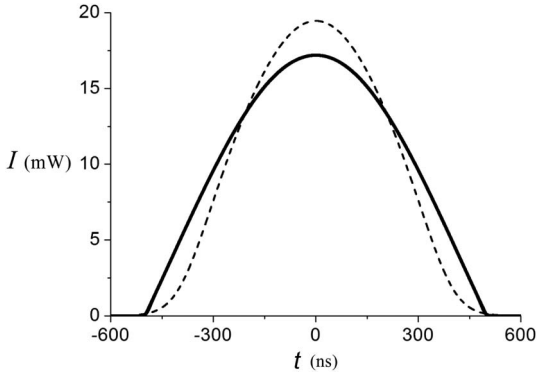

Fig. 6. Temporal intensity distribution of the laser pulse at the start of the transient process $\zeta = 3$ (dashed curve) and after the stationary distribution was reached ($\zeta = 100$, $\zeta = 10^3$, $\zeta = 10^4$, $\zeta = 10^5$, bold curve), $a = 0.80$.

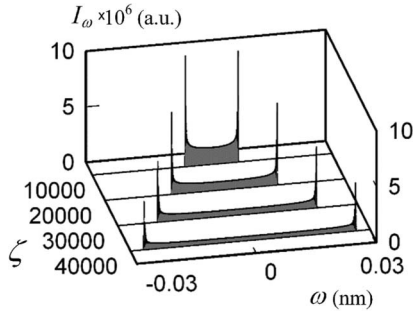

Fig. 7. Fragment of the spectral evolution of the laser pulse I_ω as a function of the number of trips around the cavity ζ(transient process). Laser parameters are the same as in Fig. 6.

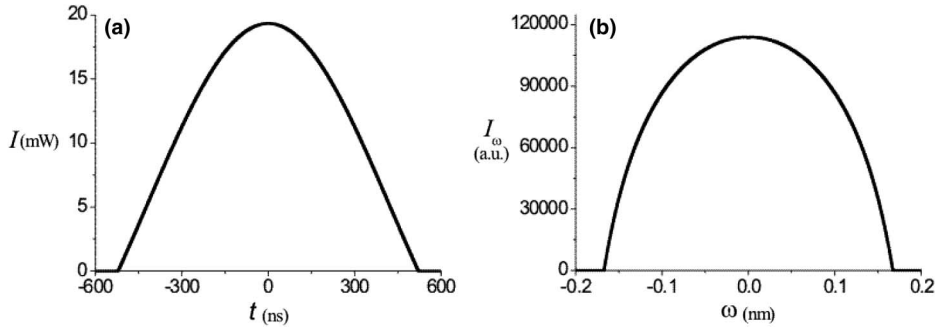

Fig. 8. (a) Temporal and (b) spectral intensity distribution of the laser pulse in the steady-state generation regime at $a = 0.85$.

The pump parameter a was chosen so as to match the experimental output intensity equal to 1 mW. The product of the pulse duration (in seconds at half-peak intensity) and its spectral width (in hertz) amounts to $\sim 10^4$.

The transient evolution of the temporal intensity distribution demonstrated in Fig. 6 is typical for the studied hybrid semifiber laser with synchronous pumping. The observed peculiarities of the spectral evolution presented in Fig. 7 are related to the following circumstance. After each new cavity round trip, an extra phase incursion is introduced along the front and rear edges of the pulse equal to qI_p. This leads to frequency change by $2qI_p/\tau_p$, where τ_p and I_p are the duration and peak pulse intensity, respectively. Therefore, for the front and rear wings of the pulse, we obtain the following evolution of the carrier frequency corresponding to the spectral peaks of Fig. 7:

$$\omega \approx \pm \frac{2qI_p}{\tau_p} N, \tag{4}$$

where N is the number of the field round trips over the cavity. Limits to the spectrum broadening that lead to settling into a steady-state spectral distribution are related to finite filter bandwidth and also to frequency dispersion of the fiber refractive index. Let us estimate the value of the spectral width for the second case of limitation. Frequency increment $\delta\omega$ over one round trip equals $\delta\omega = 2qI_p/\tau_p$. At the same time, the frequency decrement from dispersion spreading of the pulse is given by the expression $\omega\delta\tau_p/\tau_p$. In case of a stationary equilibrium pulse, these processes have to cancel out. Therefore, equating the corresponding terms, we obtain the stationary values of carrier frequency in the pulse wings:

$$\omega_s \approx \pm \sqrt{\frac{qI_p}{|D_i|}}. \tag{5}$$

In derivation of Eq. (5), we took into account that $\delta\tau \approx 2D_i\omega$. From Eqs. (4) and (5) we can derive the formula for the number of cavity round trips needed to reach the stationary state:

$$N_s \approx \frac{\tau_p}{2\sqrt{|D_i| qI_p}}. \tag{6}$$

The results of numerical modeling for the width of the generated spectrum and duration of the transient process match by the order of magnitude the calculations according to estimations in Eqs. (4)–(6).

For utilized model parameters and selected pump power ($a = 0.85$, see Fig. 8), we calculated the pulse duration to be $\tau_p = 0.66$ μs, peak intensity $I_p = 19$ mW, average intensity of the output radiation $\bar{I} = 1$ mW ($\bar{I} = I_p\tau_p/T_a$, where T_a is the cavity round-trip time). These data are in good agreement with the experiment results (to the precision of ~10%). However, the spectral width of the generated pulse in the simulated stationary-state operation was 0.26 nm, which is approximately twice as narrow as the experimental value. This mismatch is likely arising from error in values of the nonlinearity parameter and frequency dispersion of the refractive index of the cavity fiber. It may be also noted that our numerical model does not include current-dependent dynamics of dispersion and nonlinearity in the SOA. However, variation of these parameters in the SOA, whose chip length is just 1.5 mm, does not affect appreciably the dynamics of relatively long pulses generated in the fiber cavity, whose length exceeds 2 km. This relation between the active medium length and that of the cavity leads to overwhelming domination of the cavity dispersion and nonlinear properties over those of the active medium. Therefore, it can be concluded that the numerical modeling corroborates the key properties of pulses generated in a hybrid semifiber laser.

4. CONCLUSION

This work has for the first time demonstrated the possibility of mode locking in a hybrid SOA-fiber laser realized through synchronous pumping by gain modulation of an SOA used in such a laser as the active medium. When the SOA was pumped with electric current pulses having a duration of 1.2 μs (the duration was limited by available electronics), the duration of generated pulses amounted to 650 ns at the average output power of 1 mW and the pulse energy of 12 nJ. Duration of laser pulses in the proposed mode-locking method can be further reduced by using shorter current pump pulses driving the SOA, by taking into account fast SOA response time (tens of picoseconds) and its relatively broad spectral working range. The presented results of numerical modeling are close to the experimentally observed ones and corroborate the feasibility of the proposed mode-locking method in hybrid SOA fiber lasers.

Funding. Russian Science Foundation (RSF) (17-12-01281).

Acknowledgment. A. K. Dmitriev acknowledges support from the Ministry of Education and Science of the Russian Federation for his modeling work in frame of the state task No. 3.6835.2017/8.9.

REFERENCES

1. P. Paulus, R. Langenhorst, and D. Jager, "Generation and optimum control of picosecond optical pulses from gain-switched semiconductor lasers," IEEE J. Quantum Electron. **24**, 1519–1523 (1988).
2. J. J. Zayhowski, J. Ochoa, and A. Mooradian, "Gain-switched pulsed operation of microchip lasers," Opt. Lett. **14**, 1318–1320 (1989).
3. R. P. Davey, K. Smith, R. Wyatt, D. J. Williams, M. J. Holmes, D. M. Pataca, M. L. Rocha, and P. Gunning, "Subpicosecond pulse generation from a 1.3 μm DFB laser gain-switched at 1 GHz," Electron. Lett. **32**, 349–350 (1996).
4. A. S. Avtukh, N. I. Zhavoronkov, and V. P. Mikhailov, "Efficient chromium-doped forsterite laser with gain switching," Quantum Electron. **27**, 129–131 (1997).
5. Y. Kusama, Y. Tanushi, M. Yokoyama, R. Kawakami, T. Hibi, Y. Kozawa, T. Nemoto, S. Sato, and H. Yokoyama, "7-ps optical pulse generation from a 1064-nm gain-switched laser diode and its application for two-photon microscopy," Opt. Express **22**, 5746–5753 (2014).
6. O. Svelto, *Principles of Lasers*, 5th ed. (Springer, 2010).
7. C. Gua, L. Xu, W. H. Chung, L. Shao, H. Y. Tam, and H. Ming, "Gain switching of an Yb-doped DFB fiber laser," Proc. SPIE **6838**, 683808 (2007).
8. M. Giesberts, J. Geiger, M. Traub, and H.-D. Hoffmann, "Novel design of a gain-switched diode-pumped fiber laser," Proc. SPIE **7195**, 71952P (2009).
9. V. Agrež and R. Petkovšek, "Gain switch laser based on microstructured Yb-doped active fiber," Opt. Express **22**, 5558–5563 (2014).
10. M. Jiang and P. Tayebati, "Stable 10 ns, kilowatt peak-power pulse generation from a gain-switched Tm-doped fiber laser," Opt. Lett. **32**, 1797–1799 (2007).
11. F. Wang, D. Shen, H. Chen, D. Fan, and Q. Lu, "Modeling and optimization of stable gain-switched Tm-doped fiber lasers," Opt. Rev. **18**, 360–364 (2011).
12. X. Cheng, Z. Li, J. Hou, and Z. Liu, "Gain-switched monolithic fiber laser with ultra-wide tuning range at 2 μm," Opt. Express **24**, 29126–29137 (2016).
13. R. Paschotta, J. Nilsson, P. R. Barber, J. E. Caplen, A. C. Tropper, and D. C. Hanna, "Lifetime quenching in Yb-doped fibres," Opt. Commun. **136**, 375–378 (1997).
14. M. Nakandakari, K. Kuroda, and Y. Yoshikuni, "Metastable-state lifetime of erbium ions measured in the fiber propagation direction: expansion of measurable fiber length," Jpn. J. Appl. Phys. **56**, 112501 (2017).
15. T. Hessler, S. Haacke, J. L. Pleumeekers, P. E. Selbmann, M. A. Dupertuis, B. Deveaud, R. A. Taylord, P. Doussière, M. Bachmann, T. Ducellier, and J. Y. Emery, "Time-resolved relaxation oscillations in gain-clamped semiconductor optical amplifiers by pump and probe measurements," J. Opt. B **9**, 675–680 (1997).
16. K. Morito, S. Tanaka, S. Tomabechi, and A. Kuramata, "A broad-band MQW semiconductor optical amplifier with high saturation output power and low noise figure," IEEE Photon. Technol. Lett. **17**, 974–976 (2005).
17. K. Morito and S. Tanaka, "Record high saturation power (+22 dBm) and low noise figure (5.7 dB) polarization-insensitive SOA module," IEEE Photon. Technol. Lett. **17**, 1298–1300 (2005).
18. M. Haridim, B. I. Lembrikov, and Y. Ben-Ezra, *Advances in Optical Amplifiers* (InTech, 2011), Chap. 1.
19. E. V. Andreeva, S. N. Il'chenko, M. A. Ladugin, A. A. Lobintsov, A. A. Marmalyuk, M. V. Shramenko, and S. D. Yakubovich, "Broadband semiconductor optical amplifiers of the spectral range 750–1100 nm," Quantum Electron. **43**, 994–998 (2013).
20. K. Tamura, E. P. Ippen, and H. A. Haus, "Optimization of filtering in soliton fiber lasers," IEEE Photon. Technol. Lett. **6**, 1433–1435 (1994).
21. A. Komarov, H. Leblond, and F. Sanchez, "Multistability and hysteresis phenomena in passively mode-locked fiber lasers," Phys. Rev. A **71**, 053809 (2005).
22. T. Hansson and S. Wabnitz, "Frequency comb generation beyond the Lugiato-Lefever equation: multi-stability and super cavity solitons," J. Opt. Soc. Am. B **32**, 1259–1265 (2015).
23. T. R. Taha and M. J. Ablowitz, "Analytical and numerical aspects of certain nonlinear evolution equations. II. Numerical, nonlinear Schrödinger equation," J. Comput. Phys. **55**, 203–230 (1984).
24. J. C. Butcher, *Numerical Methods for Ordinary Differential Equations* (Wiley, 2008).